J. Math. Biol. (2004)
Digital Object Identifier (DOI):
10.1007/s00285-004-0270-x

Mathematical Biology

David A. Edwards*

Refining the measurement of rate constants in the BIAcore

Received: 6 January 2003 / Revised version: 1 August 2003 /
Published online: 23 April 2004 –

Abstract. When estimating rate constants using the BIAcore surface plasmon resonance (SPR) biosensor, one must have an accurate mathematical model to interpret sensogram data. Several models of differing complexity are discussed, including the effective rate constant (ERC) approach. This model can be shown formally to be good within $O(\mathrm{Da})$ in the limit of small Damköhler number Da, which is the ratio of the reaction rate to the rate of transport to the surface. Numerical results are presented that show that except for very slow reactions, parameter estimates from the ERC model are very close to those estimated using a more complicated model. The BIAcore measures the behavior of an evanescent wave whose signal strength decays as it penetrates into the device. It is shown that this decay does not appreciably affect the sensogram readout at low Da, but at moderate Da can lead to situations where two vastly different rate constants can produce the same short-time sensogram data.

1. Introduction

A necessary part of understanding many biological processes is the determination of the speed at which the underlying biochemical reactions occur. Thus, scientists need ways to estimate accurately the *rate constants* for any given reaction. Such measurements can be most readily obtained from real-time measurements of the species evolution for a particular reaction. One popular device for obtaining such data is the BIAcore, which is a surface plasmon resonance (SPR) device.

The configuration of the BIAcore is described in great detail elsewhere [17, 18, 20, 32]. We present a brief review for our purposes (see Fig. 1). The BIAcore device consists of a rectangular channel through which one of the reactants (the *analyte*) is convected in standard two-dimensional Poiseuille flow from $x = 0$, the inlet position. The other reactant (the *receptor*) is embedded in a thin dextran matrix attached to the ceiling of the channel.

Clearly the BIAcore does not replicate systems where two reactants are mixed in solution. Regardless, many bimolecular biochemical reactions of interest occur between a reactant confined to a thin layer about a surface and one floating freely

D.A. Edwards: Department of Mathematical Sciences, University of Delaware, Newark, DE 19716-2553, USA. e-mail: edwards@math.udel.edu

Mathematics Subject Classification (2000): 35B20, 35C15, 35K60, 45J05, 92C45

Key words or phrases: Biomolecular reactions – Rate constants – Asymptotics – Integro-differential equations – Dextran layer – Evanescent wave – BIAcore

* This work was supported in part by NIGMS Grant 1R01GM067244-01.

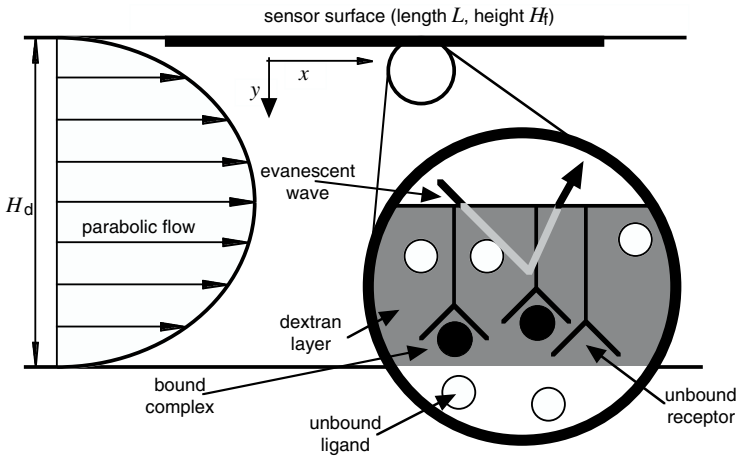

Fig. 1. Schematic of the BIAcore device.

in solution. Models for blood clotting treat the vessel as a reacting wall [1]. Drugs related to distamycin bind to reacting sites on the surface of a much larger DNA molecule [19]. Immunoglobulins are transmitted to newborns from mother's milk through binding to receptors on intestinal epithelial cells [27]. Cytoplasmic signaling and adapter molecules interact with the cytoplasmic tails of receptors embedded in the plasma membrane [13]. Antibodies bind to chemokine receptors in the surface-volume geometry [15]. Gene expression is significantly influenced by DNA-protein interactions in these geometries [32].

To measure binding in the BIAcore, an evanescent wave is bounced off the channel ceiling and read by a detector. As the experiment progresses, binding causes analyte molecules to dislodge solvent molecules. Since the analyte and solvent have different indices of refraction, binding causes refractive changes to the polarized light beam. These changes, when compared to a control state, can be translated into a *sensogram* of the binding [10]. The strength of the beam decays as it penetrates into the dextran layer [17,20,28], and so reactions occuring closer to the channel ceiling will be weighted more strongly than those near the dextran-flow interface. The sensogram data is then transferred to a regression program which predicts the rate constants using an appropriate mathematical model.

In the next section, we summarize several models used to obtain rate constants, then examine two cases in detail. First, we compare a simple ordinary differential equation (ODE) model (that contains many assumptions about the device) with a more precise (and more complicated) integrodifferential equation (IDE) model. Previous analyses [8] have shown that the predicted bound-state profiles from the two models compare favorably. However, for experimental purposes parameter estimates are more useful, so in this work we compare the rate constant estimates from the two models. The parameter estimates from the simpler model compare favorably with those of the IDE model in all but the slowest reactions.

Second, we expand previous analyses to include the effect of evanescent wave decay, and its incumbent weighting of the reaction signal depending on distance from the channel ceiling. In most experimental cases the effect of wave decay is insignificant. Nevertheless, in transport-limited cases the *same* short-time sensogram data can be generated by two different sets of rate constants via the same model, making such data useless for parameter estimation.

2. Various mathematical models

We first examine the standard evolution equation governing the evolution of the bound state $\tilde{B}$ (the tilde notation refers to variables with units). In the BIAcore, the equation is given by

$$\frac{\partial \tilde{B}}{\partial \tilde{t}} = k_{\mathrm{a}}(C_{\mathrm{T}} - \tilde{C}_{\Delta})(R - \tilde{B}) - k_{\mathrm{d}}\tilde{B}, \tag{1}$$

where k_{a} and k_{d} are the association and dissociation rate constants, R is the initial number of empty receptor sites, and $\tilde{C}_{\Delta}$ is the deviation of the analyte from the inlet concentration C_{T}. Thus in order to estimate rate constants from BIAcore sensograms, one must have an accurate mathematical model for the dynamics in the device in order to determine $\tilde{C}_{\Delta}$. We summarize three major categories of models below; they are listed in decreasing order of complexity.

2.1. Partial differential equation (PDE) models

In order to capture every detail of $\tilde{C}_{\Delta}$ in the BIAcore accurately, one must solve a convection-diffusion PDE in the bulk flow, which is assumed to be standard channel flow in the $\tilde{x}$-direction [3]:

$$\frac{\partial \tilde{C}_{\Delta}}{\partial \tilde{t}} = D_{\mathrm{f}}\left(\frac{\partial^2 \tilde{C}_{\Delta}}{\partial \tilde{x}^2} + \frac{\partial^2 \tilde{C}_{\Delta}}{\partial \tilde{y}^2}\right) - V\frac{\tilde{y}}{H_{\mathrm{f}}}\left(1 - \frac{\tilde{y}}{H_{\mathrm{f}}}\right)\frac{\partial \tilde{C}_{\Delta}}{\partial \tilde{x}}, \tag{2a}$$

where V is four times the maximal velocity in the channel, D_{f} is the diffusion coefficient of the analyte in the flow, and H_{f} is the height of the flow cell. This is usually done numerically, often with the reacting zone being treated as a boundary condition where the flux balances [2,11,25]:

$$-D_{\mathrm{f}}\frac{\partial \tilde{C}_{\Delta}}{\partial \tilde{y}}(\tilde{x}, 0, \tilde{t}) = \frac{\partial \tilde{B}}{\partial \tilde{t}}. \tag{2b}$$

Alternatively, one may treat the reacting zone as a separate layer in which the following reaction-diffusion PDE must be solved [28]:

$$\frac{\partial \tilde{C}_{\Delta}}{\partial \tilde{t}} = D_{\mathrm{d}}\left(\frac{\partial^2 \tilde{C}_{\Delta}}{\partial \tilde{x}^2} + \frac{\partial^2 \tilde{C}_{\Delta}}{\partial \tilde{y}^2}\right) + \frac{\partial \tilde{B}}{\partial \tilde{t}}, \tag{3}$$

where D_{d} is the diffusion coefficient in the reacting zone, which is often made of dextran. In either case, the numerical solution thus obtained for the bound state $\tilde{B}$ can be averaged over the appropriate region to provide data which can be compared with sensograms.

2.2. Integrodifferential equation (IDE) models

In most BIAcore experiments, convective effects dominate diffusive effects: this is indicated by the presence of a large Peclét number Pe, which measures the ratio of a characteristic diffusion time to a characteristic convection time. Typical BIAcore experiments have $\mathrm{Pe} = O(10^2)$ [3]. Thus, the dominant contribution to the reaction comes from the concentration in the unstirred Lévêque boundary layer near the flow-dextran interface [1,3,33]. In the boundary layer, one may simplify Eq. (2a) to obtain a PDE that can be solved using Laplace transforms. Using this fact, an explicit expression for the solution to the convection-diffusion equation may be constructed to within $O(\mathrm{Pe}^{-1})$ [3].

When the receptor layer is treated as a surface, the solution to Eqs. (2) for $\tilde{C}_\Delta$ is then given by [8]

$$\tilde{C}_\Delta(x,\tilde{t}) = \left(\frac{H_\mathrm{f}}{3VD_\mathrm{f}^2}\right)^{1/3} \frac{1}{\Gamma(2/3)} \int_0^x \frac{\partial \tilde{B}}{\partial \tilde{t}}(x-\xi,\tilde{t}) \frac{d\xi}{\xi^{2/3}}, \tag{4}$$

where $\Gamma(\cdot)$ is the gamma function and x has been scaled by the length L of the device. Note that Eq. (4) has an elegant physical interpretation: the difference $\tilde{C}_\Delta$ between the concentration at x and the inlet concentration is given by the accumulation (integral) of the analyte used up in the reaction ($\partial\tilde{B}/\partial\tilde{t}$) upstream ($0 \le \xi \le x$). The $1/3$ scaling properties of the flow near the reacting surface [3,22] determine the form of the multiplicative factor.

The system for $\tilde{B}$ now consists of Eq. (1) coupled to the nonlinear IDE Eq. (4); hence we denote such models as IDE models. Due to the large value of Pe, which renders this approximation extremely accurate, in this work the solution to Eqs. (1) and (4) is treated as the "true" solution for $\tilde{B}$.

2.3. Ordinary differential equation (ODE) methods

Mathematically, it is often easier to work with scaled quantities rather than dimensional ones. In addition, it can simplify various sorts of parameter estimation. The technique of *global analysis* involves fitting sensograms with differing values of C_T to the same model in order to obtain more reliable estimates [25]. By using dimensionless quantities, the sensograms (now measured as a percentage of C_T) all collapse onto the *same* graph, thus providing multiple data sets for the *same* parameter fit.

When analyzing scaled quantities, the *Damköhler number* Da arises as a key parameter:

$$\mathrm{Da} = k_\mathrm{a} R L^{1/3} \left(\frac{H_\mathrm{f}}{VD_\mathrm{f}^2}\right)^{1/3} = \frac{\text{reaction rate}}{\text{diffusion rate in unstirred layer}}, \tag{5}$$

since C_Δ is proportional to it. Hence in the limit that $\mathrm{Da} \to 0$ (which corresponds to a case where transport effects are negligible), we may expand $\tilde{B}$ asymptotically as follows:

$$\tilde{B}(\tilde{x},\tilde{y},\tilde{t};\mathrm{Da}) = \tilde{B}_0(\tilde{t}) + \mathrm{Da}\tilde{B}_1(\tilde{x},\tilde{y},\tilde{t}) + O(\mathrm{Da}^2), \tag{6}$$

where the spatial uniformity of the first term arises in the physically relevant case when the initial condition for $\tilde{B}$ is spatially uniform. Upon substitution of Eq. (6) into Eq. (4), the system becomes linear [5].

Then one can solve for $\tilde{C}_\Delta$ in Eq. (4) and use the result in Eq. (1) to obtain the following *effective rate constant* approximation (ERC) that replaces Eq. (1):

$$\frac{d\langle\tilde{B}\rangle}{d\tilde{t}} = \frac{k_a C_T(R - \langle\tilde{B}\rangle) - k_d\langle\tilde{B}\rangle}{1 + (\mathrm{Da}/R)(R - \langle\tilde{B}\rangle)\langle h\rangle} + O(\mathrm{Da}^2). \tag{7}$$

Here $\langle h\rangle$ is a constant, the average of a function $h(\tilde{x}, \tilde{y})$ that contains all the secondary effects one wishes to consider, such as device geometry [7], convective and diffusive transport [2,4,6,23], receptor layer [5,34], and evanescent wave decay [30]. We shall examine several cases for $\langle h\rangle$ below.

The ERC is very useful because it is an equation for $\langle\tilde{B}\rangle$ alone. $\langle\tilde{B}\rangle$ is the average of the bound state over the region sensed by the BIAcore, and hence is directly related to the sensograms produced by the device. Also, the only value of $\tilde{C}$ needed in the ERC model is the inlet value C_T.

If $\mathrm{Da} = 0$, the denominator in Eq. (7) becomes 1 and we obtain the evolution equation for two species well-mixed in solution with a high analyte concentration. In the BIAcore, this corresponds to the limit of infinitely high velocity, which would overwhelm upstream depletion effects and keep the bulk concentration at the value C_T. Though this well-mixed approximation is occasionally used [14], in practice there will always be some effect due to transport. Thus if fitting to the well-mixed model, one would observe that the rate "constants" vary with time due to the presence of $\langle\tilde{B}\rangle$ in the denominator, a phenomenon called *multiphasic* rate constants [9].

Nevertheless, the simple form of the well-mixed equation makes keeping Da low a paramount concern in experimental design. Unfortunately, R must be maintained at a moderate level to ensure that the signal strength is well above the noise ratio; this always keeps Da above zero and in some cases can force Da to be quite large.

Some authors (for example, [18]) try to fit a subset of data near the steady state to the well-mixed approximation, theorizing that the smaller reactive fluxes near equilibrium will be less affected by transport. Schuck and Minton [30] have pointed out that this reasoning is faulty, but the fallacy may now be stated more precisely. Eq. (7) indicates that the effect of transport in the denominator remains of the same order of magnitude throughout the entire experiment. Though the *absolute* effect of transport may be small near equilibrium, in a *relative* sense the size is the same. Thus, doing a fit to the well-mixed case will not yield accurate rate constant estimates unless almost all the receptor sites are used at equilibrium, in which case $\langle\tilde{B}\rangle \approx R$ and the denominator is approximately equal to 1.

Lastly, note that the denominator of Eq. (7) may be related to the *Onsager coefficient* $\mathrm{On} = k_a(R - \tilde{B})$ [2]:

$$1 + (\mathrm{Da}/R)(R - \langle\tilde{B}\rangle)\langle h\rangle = 1 + \langle h\rangle \left(\frac{H_f L}{V D_f^2}\right)^{1/3} \langle \mathrm{On}\rangle.$$

3. Using the ERC for high Da

Equation (7) was derived (and can be proven valid) in the limit of small Da [6]. However, unlike many asymptotic formulæ, there is nothing in the form of Eq. (7) that diverges or otherwise inherently signals its breakdown when Da is not small. Due to the more complicated nature of IDE or PDE models, it would be extremely useful to establish the efficacy of the much simpler ERC in cases where $\mathrm{Da} = O(1)$. Since the analytical result can be shown only for small Da, we must rely on numerical evidence.

When the reacting zone is treated as a surface, the constant $\langle h \rangle$ in Eq. (7) is given by [8]

$$\langle h \rangle_0 = \frac{3^{5/3}(x_{\max}^{4/3} - x_{\min}^{4/3})}{4\Gamma(2/3)(x_{\max} - x_{\min})}, \tag{8}$$

where the subscript zero is added for reasons that will become clear below. Here $x_{\min}$ and $x_{\max}$ are the endpoints of the *scanning range* over which the mass changes are averaged.

Edwards and Jackson [8] compare the ERC solution $\langle \tilde{B} \rangle$ of Eq. (7) with the solution $\tilde{B}$ of Eqs. (1) and (4), averaged over the scanning range. As parameters, they use Da and a dimensionless affinity constant

$$K = \frac{k_\mathrm{d}}{k_\mathrm{a} C_\mathrm{T}} = \frac{\text{time scale for association}}{\text{time scale for dissociation}}.$$

Note from their forms that given values for K and Da, both rate constants can be determined since all the other experimental parameters are assumed known.

The authors take $K = 1$ and examine numerical simulations for a wide range of Da, each taken to steady state. The simulations were generated without noise, as any such noise would affect each model similarly. In their simulations, they establish that the *profiles* for $\langle \tilde{B} \rangle$ given by Eq. (7) and the solution $\tilde{B}$ of Eqs. (1) and (4) do not differ by more than 3%, even in the transport-limited case where $\mathrm{Da} \to \infty$. Though these results are encouraging, they do not address the central issue: Estimating the rate constants. Therefore, we examine the difference in *parameter estimates* between solutions to the ERC and IDE models.

In order to generate the results, we use the coding algorithm outlined in Edwards and Jackson [8] to solve Eqs. (1) and (4). Initially we take $K = 1$ and let Da vary. The solution thus constructed utilizes only the large Pe approximation, and hence most closely represents the true sensogram data. This solution is passed to Matlab as the experimental data, and we use the `lsqcurvefit` command to fit the data to Eq. (7). The command yields the value of Da which best fits the data.

The results are shown in Fig. 2. As expected for small values of Da, where we know the ERC to be a good approximation, the estimated value of Da is extremely close to the true value. Looking at larger values of Da, though the estimated values of Da have drifted from the true values, the percentage error is quite small—certainly within experimental tolerances. Thus after examination of Fig. 2 we may be led to conclude that the effective rate constant approximation will always provide

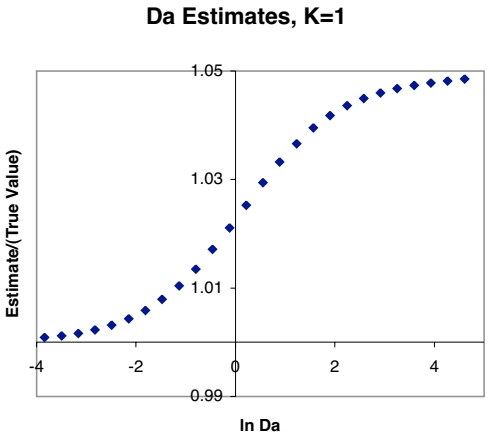

Fig. 2. Graph of the ratio of the ERC to IDE estimates of Da. The ERC estimate is calculated by using Eq. (7) as a model to the solution of Eqs. (1) and (4) with $K = 1$. The diamonds are the data points computed; they would lie on the line $y = 1$ (where the x-axis crosses) if the IDE and ERC models were identical.

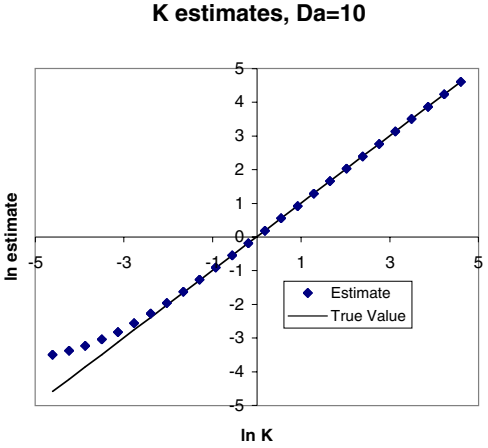

Fig. 3. Log-log graph of the estimate of K calculated by using Eq. (7) as a model to the solution of Eqs. (1) and (4) with $\mathrm{Da} = 10$. The diamonds are the data points computed; the line shows where the data points would lie if the IDE and ERC models were identical.

accurate estimates of the rate constants. Unfortunately, that is not always the case, as can be seen in Fig. 3.

In Fig. 3, we examine the case where $\mathrm{Da} = 10$. This corresponds to a case where transport effects are quite pronounced. We again generate "experimental data" using Eqs. (1) and (4) for various values of K. Then this data was fit in Matlab to Eq. (7), except in this case K was returned as the best-fit parameter. For large values of K, the estimate is again indistinguishable from the true value, and this close agreement extends to moderately small values of K. On the other hand,

for very small values of K, the estimate widely diverges from the true value. (For instance, the data point for the smallest value of K is off by a factor of 3.)

How then to explain the discrepancy between the two figures? Since transport effects slow the reaction process, an experiment with a high value of Da will take longer than one with a smaller value of Da. In addition, the percentage of receptors bound when the experiment reaches steady state is given by $(K+1)^{-1}$ [3]. Thus for a fixed value of Da (and hence k_a), varying K will vary the length of the experiment. Smaller values of K correspond to longer experiments.

A reaction where transport is important will proceed more slowly than the "ideal" case where transport is negligible. This difference in speed will accumulate over time. Thus the longer the experiment takes (as measured on the reaction time scale), the more suspect the parameter estimates should be. Since even the simplest model can provide order-of-estimate sizes for the reaction time scale, a single injection run can provide insight as to whether the ideal case estimates should be suspect.

4. The evanescent wave layer

The reacting zone in the BIAcore is actually a layer (usually receptors embedded in dextran) of width H_d. The BIAcore measures the refractive behavior of an evanescent wave that bounces off this dextran matrix. Mass changes are averaged over the scanning range, and measurements returned in terms of *response units*. Due to the nature of the instrument, the signal decays with distance from the ceiling of the device (see Fig. 1).

The presence of the dextran layer affects the transport process, hindering diffusion to reacting sites. This effect can be exacerbated by the decay length of the wave layer. One can envision a very poorly designed experiment where the dextran layer is thick and presents a high barrier to diffusion. In such an experiment, the binding would occur in a thin zone about the dextran-flow interface. If the wave decays quickly compared to the dextran thickness, it would not reach the area where binding had occurred, and the sensogram would show few response units. Clearly this is an extreme case, but in the remaining sections we quantify the decay effects more precisely. In this way, we can determine when it is necessary to include these effects in the analysis of an experiment.

We work with scaled variables, which we denote without tildes. We scale the analyte concentration by C_T and the bound state by R. (Here we have assumed the initial receptor density to be uniform in x and y; further remarks on this point may be found in the discussion section.) Lengths in the y-direction (normal to the flow) are scaled by H_d, and $y = -1$ is taken to be the channel ceiling.

Since our work here concerns the effectiveness of the sensogram *measurement* of the binding, rather than the actual binding itself, we refer readers interested in those details to Edwards' work [5] on the binding in a receptor layer. With these scalings, Eq. (3) becomes

$$\frac{\partial^2 C_\Delta}{\partial y^2} = -\mathrm{Da} D \frac{\partial B_d}{\partial t}, \tag{9a}$$

$$D = \frac{D_f/(H_f \mathrm{Pe}^{-1/3})}{\phi D_d/H_d} = \frac{\text{diffusion "velocity" in diffusive boundary layer}}{\text{diffusion "velocity" in dextran}}, \quad (9b)$$

where ϕ is the partition coefficient. Here D is a dimensionless parameter that characterizes the effect of the dextran on diffusion; $D = 0$ corresponds to reaction on a surface.

Then by introducing a new function F, one can rewrite the expression for C_Δ as [5]

$$C_\Delta(x, y, t) = -\mathrm{Da}\left[DF - \frac{1}{3^{1/3}\Gamma(2/3)} \int_0^x \frac{\partial F}{\partial y}(x - \xi, 0, t) \frac{d\xi}{\xi^{2/3}}\right], \quad (10a)$$

$$\frac{\partial^2 F}{\partial y^2} = \frac{\partial B}{\partial t}, \qquad \frac{\partial F}{\partial y}(x, -1, t) = 0, \qquad F(x, 0, t) = 0. \quad (10b)$$

Here the second term in the bracketed equation is a function of only x and t chosen to satisfy the boundary conditions.

For the decay rate $\mathcal{K}(y)$ of the wave, we postulate the simplest possible form, namely

$$\mathcal{K}(y) = \mathrm{e}^{-\delta(y+1)}, \qquad \delta = H_d/H_w, \quad (11)$$

where H_w is the *penetration depth* of the wave, which ranges between 1 and 2×10^{-5} cm [17,20,28].

δ is the key parameter in this analysis, as it measures the effect of the decay. Here $\delta = 0$ corresponding to a wave that propagates infinitely far into the device. Since this corresponds to perfect averaging over the entire receptor layer, we call this the "perfect case". Since the height of the dextran layer in the standard CM5 chip is about 10^{-5} cm [26], δ is typically between 0.5 and 1. See the Appendix for a fuller range of experimentally realizable values of δ.

Using our expression for $\mathcal{K}(y)$ given in Eq. (11), the averaging takes the following form:

$$\langle \tilde{B} \rangle(t) = \mathcal{K}_0 R \int_{x_{\min}}^{x_{\max}} \int_{-1}^{0} \mathrm{e}^{-\delta(y+1)} B(x, y, t)\, dy\, dx,$$
$$\mathcal{K}_0 = \frac{\delta}{(1 - \mathrm{e}^{-\delta})(x_{\max} - x_{\min})}, \quad (12)$$

where $\langle \tilde{B} \rangle$ is now the sensogram response. Here $\mathcal{K}_0$ is a normalization factor which ensures that $\langle a \rangle = a$ for any constant a. By taking $\delta \neq 0$, the effects of decay are included. We now examine the deviation of the $\delta \neq 0$ case from the perfect case where $\delta = 0$.

5. Small Da

5.1. Explicit solution

In this section we specialize to the case where the initial state for B is the constant value zero. Thus we may expand our expression for B as in Eq. (6). Since B_0 is

uniform in x and y, it is unaffected by the wave decay. We may also expand F in a perturbation series in Da. These expansions linearize Eq. (10a), which allows us to write B_1 as [5]

$$B_1(x, y, t) = -\frac{e^{-\alpha t}}{\alpha}\left(\frac{e^{-\alpha t}-1}{\alpha} - Kt\right)\left\{D\left[\frac{y(y+2)}{2}\right] - \frac{3^{2/3}x^{1/3}}{\Gamma(2/3)}\right\}, \quad (13)$$

where $\alpha = K + 1$.

One can verify that the coefficient of the braced term is positive; hence the y-dependent term shows that the concentration of the bound state at the channel ceiling $y = -1$ is smaller than at the flow interface $y = 0$. This is consistent with the result that diffusion is slowing transport through the dextran layer.

To examine the sensogram data, we average the y-dependent term including the δ-term using Eq. (12) and obtain

$$\left\langle \frac{y(y+2)}{2} \right\rangle = -p(\delta), \qquad p(\delta) = \frac{\delta^2 + 2[(\delta+1)e^{-\delta} - 1]}{2\delta^2(1-e^{-\delta})}. \quad (14)$$

It can be shown that $p(\delta) \sim (1/3) + (\delta/24)$ as $\delta \to 0$, so the decay effect is $O(\delta)$ as $\delta \to 0$. Moreover, it can be shown that $1/3 \leq p(\delta) < 1/2$, which is a very narrow range. Thus we do not expect evanescent wave decay to have much effect upon the sensogram in this case.

Averaging Eq. (13) using Eq. (14), we have the following:

$$\langle B_1\rangle(t;\delta) = \frac{e^{-\alpha t}}{\alpha}\left(\frac{e^{-\alpha t}-1}{\alpha} - Kt\right)[Dp(\delta) + \langle h\rangle_0], \quad (15)$$

where we include the δ to indicate explicitly the fact that we are considering the wave decay in our analysis. In order to verify our hypothesis that the solution does not vary appreciably with δ, we generate plots using the parameters listed in Table 1.

Figure 4 shows a graph of the difference between the first-order correction $\langle B_1\rangle(t;\delta)$ (including wave decay) and $\langle B_1\rangle(t;0)$ (ignoring wave decay) for various values of δ. The range of δ is justified in the Appendix. Note the very small scale on the y-axis, confirming that for small Da the effect of wave decay is negligible. Note that as δ increases, the effect due to transport is magnified, as the averaging doesn't include the whole dextran layer evenly. Also, the difference is always negative, as the wave decay will always cause a smaller response unit reading.

Table 1. Parameters for Figs. 4 and 5. The value of D comes from the Appendix; all others come from [5].

Parameter	Value	Parameter	Value
C_T (mol/cm^3)	10^{-11}	t	$10^{-3}\,\tilde{t}$/s
D	1.20×10^{-1}	x_{max}	7.92×10^{-1}
Da	10^{-1}	x_{min}	2.08×10^{-1}
K	1	α	2
$\tilde{k}_{on}$ (cm^{3}mol^{-1}s^{-1})	10^8		

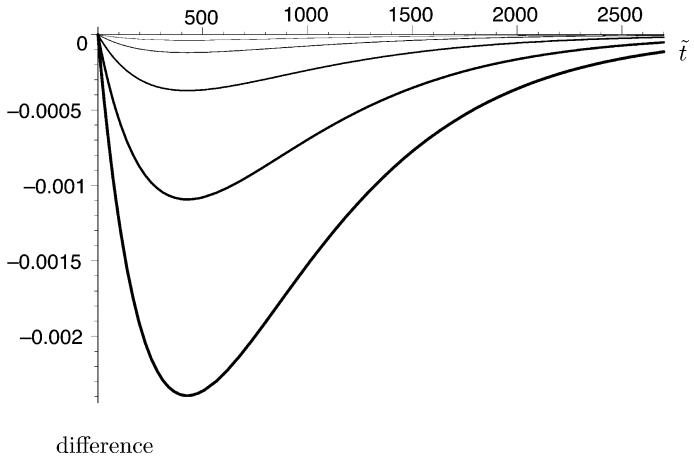

Fig. 4. The y-axis shows the difference between the solution $\langle B_1\rangle(t;\delta)$ including the wave decay and the solution $\langle B_1\rangle(t;0)$ ignoring it. The lines are for (in increasing order of thickness) $\delta = 0.05, 0.16, 0.5, 1.6$, and 5.

5.2. Effective rate constant solution

Next we turn our attention to obtaining results from the ERC model. Again, we are considering only the averaging so we may use the results from Edwards [5]. Since in the small Da case the leading order of B is spatially uniform by Eq. (6), to solve for h we essentially solve the operator in Eq. (9a) with a constant right-hand side. To aid comprehension, in this paper we have changed the sign convention to indicate that the denominator is always larger than 1 because transport slows the reaction. Thus when quoting the result from [5] we change the sign of h to obtain

$$h(x, y) = -D\left[\frac{y(y+2)}{2}\right] + \frac{3^{2/3}x^{1/3}}{\Gamma(2/3)},$$

where the Da term on the right-hand side of Eq. (9a) is accounted for in the denominator of Eq. (7).

Thus upon averaging we have the following:

$$\langle h\rangle(\delta) = Dp(\delta) + \langle h\rangle_0, \tag{16}$$

which is exactly the bracketed quantity in Eq. (15). Note that $\langle h\rangle = \langle h\rangle_0$ when $D = 0$: hence the subscript. Because of the small variance in $p(\delta)$, we again expect little change in our solutions for various values of δ. We verify this with the plots in Fig. 5.

Figure 5 shows a graph of the difference between the ERC solution $\langle B\rangle(t;\delta)$ (including wave decay) and $\langle B\rangle(t;0)$ (ignoring wave decay) for various values of δ. The scale on the y-axis is even smaller, since now the effect of the small Da has also been plotted. Thus, we see the neglibility of the decay effect for small Da. Again increasing δ causes a larger negative difference in the sensogram reading.

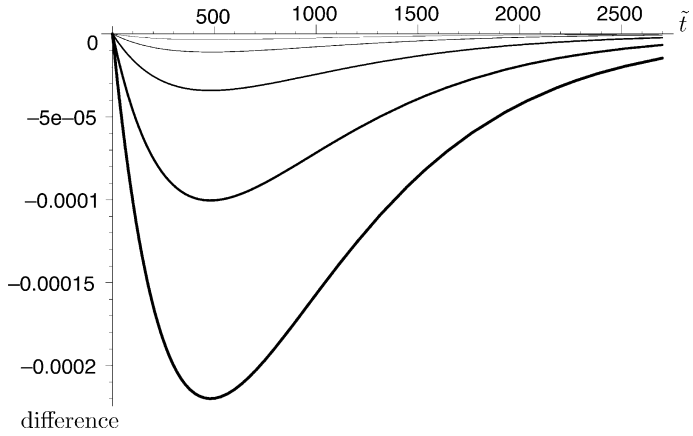

Fig. 5. The y-axis shows the difference between the solution $\langle B\rangle(t;\delta)$ of Eqs. (7) and (16) including the wave decay and the solution $\langle B\rangle(t;0)$ ignoring it. The lines are for (in increasing order of thickness) $\delta = 0.05, 0.16, 0.5, 1.6$, and 5.

6. Moderate Da

In the case of moderate Da, the IDE model now encompasses three equations: Eqs. (1) and (10). The equations are coupled in a nonlinear fashion and hence cannot be solved explicitly. Since we now have no small parameter with which to linearize our equations, we turn instead to a small *variable*, namely t.

In particular, we let $B(x, y, t) \sim \beta(x, y)t$ for small (dimensionless) t. With the scalings in [5], this implies that the dimensional time $\tilde{t} \ll (k_a C_T)^{-1}$. (Again, an order-of-magnitude estimate of k_a can be obtained with even the simplest well-mixed model.) With this assumption, $F(x, y, t) \sim F_1(x, y)$. Thus F can be replaced with F_1 in Eq. (10a), and Eq. (10b) becomes

$$\frac{\partial^2 F_1}{\partial y^2} = \beta, \qquad \frac{\partial F_1}{\partial y}(x, -1) = 0, \qquad F_1(x, 0) = 0. \tag{17}$$

Substituting Eqs. (10a) and (17) into the dimensionless form of Eq. (1) and matching the leading-order terms, we obtain

$$1 - \frac{\partial^2 F_1}{\partial y^2} = \mathrm{Da}\left[\frac{1}{3^{1/3}\Gamma(2/3)}\int_0^x \frac{\partial F_1}{\partial y}(x-\xi, 0)\frac{d\xi}{\xi^{2/3}} - DF_1\right]. \tag{18}$$

The solution process for Eq. (18) is as follows. By taking Laplace transforms, one can write Eq. (18) as an ODE for $\hat{F}_1$, the Laplace transform of F_1, which includes the boundary condition $\mathrm{d}\hat{F}_1/\mathrm{d}y(0)$ as a parameter. We solve the resulting equation and substitute the result into Eq. (17) to obtain $\hat{\beta}$, the Laplace transform of β:

$$\begin{aligned} \hat{\beta} &= \frac{1}{s}\frac{\cosh\lambda(y+1)}{\cosh\lambda}\left(1 + \frac{\mu^{1/3}}{s^{1/3}}\right)^{-1}, \\ \mu &= \frac{1}{3}\left[\frac{\mathrm{Da}\Gamma(1/3)\tanh\lambda}{\Gamma(2/3)\lambda}\right]^3, \qquad \lambda^2 = D\mathrm{Da}. \end{aligned} \tag{19}$$

Thus the leading-order variance in y is no longer parabolic as in Eq. (13), but is now in the form of a hyperbolic function.

With this short-time asymptote of the data, we may fit rate constants by examining the slope of the sensogram near $t = 0$. Then $\langle \tilde{B} \rangle (\tilde{t}) \sim RS\tilde{t}$, where [5]

$$S = \frac{k_a C_T \{\mathcal{I}[\bar{\beta}; x_{max}] - \mathcal{I}[\bar{\beta}; x_{min}]\}}{x_{max} - x_{min}}, \qquad \mathcal{I}[\bar{\beta}; x] = \int_0^x \bar{\beta}(\xi)\, d\xi. \tag{20}$$

In Eq. (20) the averaging has been done in two steps. $\bar{\beta}$ represents the average of β in the y-direction only, while the actual fraction with the $\mathcal{I}$ operator performs the averaging in the x-direction.

With the hyperbolic form of $\hat{\beta}$, the y-averaging is more complicated, producing the following result for $\mathcal{I}[\bar{\beta}; x]$:

$$\mathcal{I}[\bar{\beta}; x] = \frac{e^{-\mu x}}{\mu} \frac{f(\lambda, \delta)}{2 \cosh \lambda} \left[e^{\mu x} - 1 - |P(4/3, -\mu x)| + |P(5/3, -\mu x)| \right], \tag{21a}$$

$$f(\lambda, \delta) = \frac{\delta}{1 - e^{-\delta}} \left[\frac{e^{(\lambda - \delta)} - 1}{\lambda - \delta} - \frac{e^{-(\lambda + \delta)} - 1}{\lambda + \delta} \right], \tag{21b}$$

where P is the normalized incomplete gamma function. It can be shown that $f(\lambda, \delta) = (2 \sinh \lambda)/\lambda + O(\delta)$ as $\delta \to 0$. Thus the correction is $O(\delta)$ as $\delta \to 0$, just as in the small Da case.

Using the small- and large-μ behavior of the P function, the small- and large-k_a behavior of S can be ascertained. For small k_a, we obtain

$$S \sim k_a C_T, \qquad k_a \to 0. \tag{22a}$$

In this case, the effect of δ is negligible because the reaction is infinitely slow. Thus, the ligand concentration in the dextran layer always has time to become uniform before the reaction occurs.

On the other hand, for large k_a, we have the following:

$$S \sim \left[\frac{3^{4/3} C_T V^{1/3} D_f^{2/3} (x_{max}^{2/3} - x_{min}^{2/3})}{2\Gamma(1/3) R L^{1/3} H_f^{1/3} (x_{max} - x_{min})} \right] \frac{\delta e^{-\delta}}{1 - e^{-\delta}}, \quad k_a \to \infty. \tag{22b}$$

As $\delta \to 0$, the last fraction tends to 1, which provides a correction to Edwards [5], Eq. (72b). The presence of a finite asymptote for S in the limit of large k_a is physically reasonable, since no matter how fast the reaction proceeds, the mass uptake will be limited by the amount of unbound ligand available for assimilation. Note also that both of Eqs. (22) are independent of D.

In the case of an infinitely-fast reaction, the wave decay has substantial influence, since the term $\delta e^{-\delta}/(1 - e^{-\delta})$ quickly decreases as δ increases. In the case of moderate Da and $k_a \to \infty$, there is a small reacting zone near the flow interface where all the binding occurs. As δ increases, areas near the sensor surface (away from the reacting zone) are weighted more heavily.

Thus we expect a decrease in our signal, which is illustrated in Fig. 6. In order to simplify some of the computations, we introduce the parameter k, which is simply a scaled version of k_a, in Table 2, which lists the parameters used in Fig. 6.

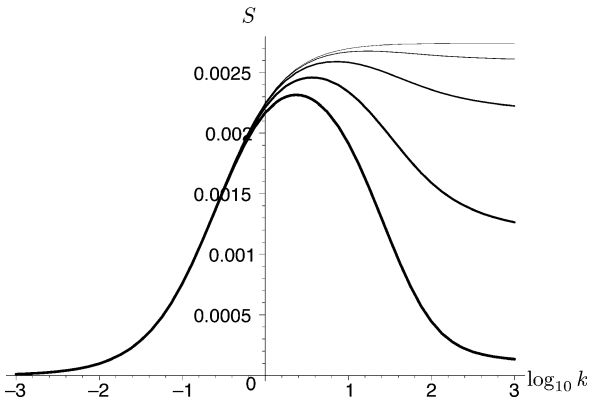

Fig. 6. *S vs.* $\log_{10} k$ for (in increasing order of thickness) $\delta = 0.05$, 0.16, 0.5, 1.6, and 5. As δ increases, the sensor cannot pick up clustering near the flow interface for high k, and the signal slope drops.

Table 2. Parameter values for Fig. 6 from [5].

Parameter	Value	Parameter	Value
C_T (mol/cm^3)	10^{-11}	R (mol/cm^2)	10^{-12}
D_f (cm^2/s)	2.8×10^{-7}	V (cm/s)	1
H_f (cm)	5×10^{-3}	x_{max}	7.92×10^{-1}
k	$10^{-9} k_a$ mol · s/cm^3	x_{min}	2.08×10^{-1}
L (cm)	2.4×10^{-1}		

Figure 6 shows *S vs. k* on a lin-log scale. Note that as δ increases, the slope of the signal curve actually has a maximum for some value of k. As k increases beyond this point, the reaction is occurring so fast that ligand molecules do not have time to diffuse closer to the channel ceiling. Though the reaction is speeding up, there is less binding *within the decay length* of the evanescent wave. Thus the slope of the signal begins to decrease, eventually going to zero at very high k_a. Since the same slope S now corresponds to two different possible values of k_a, in this case it is impossible to determine the value of the rate constants from short-time data.

Other authors have tried to estimate rate constants in the transport-limited case using a subset of the data [18]. However, there are two key differences between the approach in [18] and the one here. First, the subset taken is near the beginning of the experiment, rather than the end. More importantly, in [18] the effects of transport on the data subset are ignored. In our case, the short-time data is used because it is the *only* set that can be fit (easily) to the nonlinear model that includes transport.

Clearly the rate constants estimated from any sensogram depend on the model used; that is why the transport effects have been included in the first place. But other effects can be incorporated as well. In particular, Glaser and Hausdorf [12] and Morton et al. [24] demonstrated that incorporating the effects of conforma-

tional change into the model will significantly affect the rate constants estimated. Schuck [29] notes that non-specific binding can affect the diffusion coefficient in the dextran, thus changing the effective rate constant. Karlsson and Fält [17] showed that the same data could fit parallel, competitive, and two-state reaction models. In contrast, our result is novel because it shows that the *same* model can provide two different rate-constant estimates for the same data due to the nonuniformity of the signal response.

7. Dissociation Experiments

We now make some brief remarks regarding dissociation experiments. Assuming that the dissociation phase begins after the association phase has run to completion, the initial state for B is given by α^{-1}. In addition, the analyte is considered to be totally removed from the flow during this phase, so $C_T = 0$. Since the actual binding results are the same as in Edwards [5] and considerations of the decay length δ are exactly as above, only a brief summary is presented.

In the case of an explicit expression for small Da, we have from Eq. (76) in Edwards [5] that

$$B_1(x, y, t) = \frac{Ke^{-Kt}}{\alpha}\left(t + \frac{e^{-Kt} - 1}{K\alpha}\right)\left\{\frac{3^{2/3}x^{1/3}}{\Gamma(2/3)} - D\left[\frac{y(y+2)}{2}\right]\right\},$$

and hence using our averaging trick we obtain

$$\langle B_1\rangle(t;\delta) = \frac{Ke^{-Kt}}{\alpha}\left(t + \frac{e^{-Kt} - 1}{K\alpha}\right)\langle h\rangle(\delta),$$

which is analogous to Eq. (15). For the effective rate constant model, the only real change is that the bulk concentration of analyte is zero, so the governing equation is Eq. (7) with $C_T = 0$ and $\langle h\rangle(\delta)$ given by Eq. (16).

For the case of moderate Da, B will now be approximated by $B(x, y, t) \sim \alpha^{-1} - \beta(x, y)t$. Performing a similar analysis to the above, we obtain the following new expression for $\mathcal{I}$:

$$\mathcal{I}[\bar{\beta}; x] = -\frac{Ke^{-\mu x}}{\alpha\mu}\frac{f(\lambda,\delta)}{2\cosh\lambda}\left[e^{\mu x} - 1 - |P(4/3, -\mu x)| + |P(5/3, -\mu x)|\right],$$

where $f(\lambda, \delta)$ is given in Eq. (21b). As is true in the association case, the small k_a limit is the same whether $\delta = 0$ or not:

$$S \sim \frac{k_d}{K+1}, \qquad k_a \to 0.$$

Also, the large k_a-asymptote is provided by the $\delta = 0$ case multiplied by the same factor as in Eq. (22b):

$$S \sim \left[\frac{3^{4/3}C_T V^{1/3} D_f^{2/3}(x_{max}^{2/3} - x_{min}^{2/3})}{2\Gamma(1/3)RL^{1/3}H_f^{1/3}(x_{max} - x_{min})}\right]\frac{\delta e^{-\delta}}{(1 - e^{-\delta})}, \quad k_a \to \infty.$$

8. Discussion

To understand certain biological systems, it is vital to have accurate estimates of rate constants for the underlying chemical reactions. The BIAcore SPR device provides an excellent way to obtain real-time observations of binding processes, but such data is useless for parameter estimation without the necessary mathematical models to interpret it.

Because the receptor sites are embedded in a layer, rather than mixed in solution, such models must correctly determine $\tilde{C}_\Delta$, the deviation of the analyte concentration from the inlet (well-mixed) state. PDE models of the type illustrated in Eqs. (1)–(3) are the most accurate, but must be solved numerically. IDE systems of the type involving Eq. (1) and either Eq. (4) or Eq. (10) are less complex since each of the directions may be examined in turn, rather than together, but the resulting equations still have to be solved numerically. ODE models have the advantage of being simple to use in conjunction with standard parameter-estimation packages, but involve many assumptions.

The ERC model given in Eq. (7) can be shown to be accurate to leading two orders in the case of small Damköhler number Da [6]. By constructing experimental data using the IDE model and fitting it to the ERC equation, we showed that the rate constant estimates thus obtained are highly accurate in most cases. In Fig. 3 we showed that the only significant deviation occurs when the dimensionless affinity constant K is small and Da is moderate (a case usually avoided by experimentalists), which corresponds to a slow reaction. Thus for most practical purposes, using the ERC will produce rate constant estimates within acceptable tolerances of the true values.

Since the BIAcore uses a decaying evanescent wave to measure the kinetic process, it is clear that binding near the flow interface will be weighted less than binding near the channel ceiling. The real question from an experimental point of view is whether the decay appreciably affects the measurement of rate constants. In the case of small Da, the question need not be asked, since the ERC can be adapted using the $p(\delta)$ term to take decay into account. In addition, we demonstrated in Figs. 4 and 5 that including the effect of wave decay causes negligible differences in the binding profiles for small Da.

In this paper we assumed that the device has uniform sensitivity along the scanning range. More complicated averaging procedures modeling nonuniform sensitivity could easily be incorporated into the model if experimentally demonstrated to be necessary. However, given the relatively minor effect of the penetration depth in most cases, it seems unlikely that a nonuniform sensitivity will appreciably affect sensogram measurements.

Similarly, we assumed that the initial receptor concentration R is uniform in x and y. This assumption is more suspect, since the processes by which the receptor sites are embedded in the dextran may be susceptible to nonuniformities, and in further work we wish to consider more general cases. Nevertheless, we note that given the relatively minor effect of spatial nonuniformity demonstrated here, we expect that such considerations will not substantially affect sensogram measurements except in cases where they tend to magnify the natural spatial inhomogeneity of the binding.

In an experimental design context it is critical to keep Da as low as possible to exploit the simpler models. Unfortunately, doing so simply by increasing the flow rate will cause D, the ratio of diffusion velocities in the Lévêque layer and the dextran, to increase. This increases the effect of the dextran layer on the measurements. In addition, there is a lower bound on R that arises from maintaining enough receptor sites to guarantee a strong sensogram signal [5]. Thus it may not always be possible to keep Da small.

Unfortunately, when the Damköhler number is not small, the sensogram data may not be usable at all. Consider the following two cases. In the first, the reaction is very slow, so despite any transport effects, there is low-level binding throughout the layer, corresponding to a weak short-time sensogram response. In the second, the reaction is very fast, so significant binding occurs in a region near the flow interface, far from the channel ceiling. This still yields a weak short-time sensogram response since the binding is occurring in a region of weaker evanescent wave signal. Thus, as shown in Fig. 6, the same sensogram short-time data can correspond to two vastly different reactions.

These results demonstrate the importance of understanding the strengths and weaknesses of any model one uses for parameter estimation. Clearly the lower that one can drive the Damköhler number, the better, since then the effects of transport can be reduced. On the other hand, in cases where the Damköhler number cannot be made small, the ERC can be used in cases where δ is small. From the results in the moderate-δ, moderate-Da case, it is clear that such a set of parameters is to be avoided at all costs if accurate rate-constant estimates are to be obtained.

Nomenclature

8.1. Variables and parameters

If the same letter appears both with and without tildes, the letter with a tilde has dimensions, while the letter without a tilde is dimensionless. The equation where a quantity first appears is listed, if appropriate.

$\tilde{B}(\tilde{x}, \tilde{y}, \tilde{t})$: bound ligand concentration at position $(\tilde{x}, \tilde{y})$ and time $\tilde{t}$ (1).
C_{T}: inlet analyte concentration (1).
$\tilde{C}_{\Delta}(\tilde{x}, \tilde{y}, t)$: deviation in analyte concentration at position $(\tilde{x}, \tilde{y})$ and time $\tilde{t}$ from inlet concentration (1).
D: dimensionless parameter characterizing effect of diffusion in the dextran layer (9a).
D_{d}: diffusion coefficient of analyte in dextran (3).
D_{f}: diffusion coefficient of analyte in flow (2a).
Da: the Damköhler number, which measures the ratio of reaction and diffusion effects (5).
$F(x, y, t)$: function used in the IDE model for the receptor layer (10a).
$f(\lambda, \delta)$: function characterizing averaging in the moderate Da case (21a).
H_{d}: height of dextran layer.

H_f: height of flow channel (2a).
H_w: evanescent wave decay length (11).
$h(\tilde{x}, \tilde{y})$: function used in effective rate constant solution (7).
$\mathcal{I}\bar{\beta}; x$: integration operator, defined in Eq. (20) as

$$\mathcal{I}[\bar{\beta}; x] \equiv \int_0^x \bar{\beta}(\xi)\, d\xi.$$

$\mathcal{K}(y)$: kernel of signal measurement operator (11).
$\mathcal{K}_0$: normalization factor for signal (12).
K: dimensionless affinity constant.
k_a: association rate (1).
k_d: dissociation rate (1).
L: length of the channel.
On: Onsager coefficient.
$P(\cdot, -\mu x)$: normalized incomplete gamma function (21a).
$p(\delta)$: average of y-dependent terms (14).
Pe: Peclét number for the system.
R: initial concentration of receptor sites (1).
S: slope of sensogram data for small time (20).
$\tilde{t}$: time (1).
V: four times the (maximal) velocity of flow at center of channel (2a).
$\tilde{x}$: length along the channel (2a).
$\tilde{y}$: height from dextran-flow interface (2a).
$\mathcal{Z}$: the integers.
α: dimensionless constant, defined as $K + 1$ (13).
$\beta(x, y)$: term in expansion of $B(x, y, t)$ for small t.
$\Gamma(\cdot)$: gamma function (4).
δ: ratio of dextran width to wave decay length (11).
λ: dimensionless constant (19).
μ: dimensionless constant (19).
ξ: dummy variable (4).
ϕ: partition coefficient (9a).

Other notation

max: as a subscript, used to indicate the right endpoint of the scanning range (8).
min: as a subscript, used to indicate the left endpoint of the scanning range (8).
$n \in \mathcal{Z}$: as a subscript, used to indicate an expansion (6).
$\bar{\ }$: used to denote the mean of the bound concentration in the y-direction only (20).
$\hat{\ }$: used to indicate the Laplace transform of a quantity.
$\langle\ \rangle$: used to indicate the mean of the bound concentration in both the x- and y-directions (7).

Table 3. Parameter values from the literature.

Reference	Parameter D_d/D_f	H_d (10^{-5} cm)	H_w (10^{-5} cm)	ϕ
[9]		2–5		
[16]		1–2		
[17]			1.6	
[20]		1	1.9	
[21]		1		
[26]		0.3–1		
[28]	0.02–0.1	0.1–1	0.95	0.3–1
[31]		1–2.2		
[35]	0.04–0.12	1		0.1–0.25

Appendix

In Table 3 we compile parameter values relevant to the new analysis here; other parameters may be found in the appendices of [3,5]. The experimental values in [35] are for a bovine serum albumin/monoclonal antibody system. One may use various sensor chips of different thicknesses in the BIAcore; hence the varying values of H_d in the experimental literature. D_d/D_f, H_d, and ϕ vary in [28] because they are parameters input into numerical simulations.

To calculate the value of D in Table 1, we use the values $\mathrm{Pe} = 3.71 \times 10^2$ and $H_f = 5 \times 10^{-3}$ cm cited in [3]. For the values of D_d/D_f and ϕ, we take the largest possible upper bounds to minimize the effects of the layer. (Also, there is some dispute as to whether for all experimental setups the ratio D_d/D_f is as small as cited.) Using $D_d/D_f = 0.12$ from [35] and $\phi = 1$ from [28], we obtain the value $D = 0.12$ in Tab. 1.

With the values in [3], it can be shown that $\langle h \rangle_0 = 1.2$, an order of magnitude larger than D, and hence $\langle h \rangle_0$ is the dominant contribution to $\langle h \rangle$ in Eq. (16). This confirms the small variance in Figs. 4 and 5.

Utilizing the appropriate upper and lower bounds from the literature, we see that the possible range of values for δ is given by

$$5.26 \times 10^{-2} \leq \delta \leq 5.26,$$

which justifies the range of δ used in Fig. 6.

Acknowledgements. The author wishes to thank Seth Jackson for contributing numerical code used as a building block for the analysis in section 3. The author wishes to thank Dr. Byron Goldstein (Theoretical Biology and Biophysics Group, Los Alamos National Laboratory) for helpful discussions regarding this paper, and the referee for providing valuable suggestions.

References

1. Basmadjian, D.: The effect of flow and mass transport in thrombogenesis. Ann. Biomed. Eng. **18**, 685–709 (1990)
2. Christensen, L.L.H.: Theoretical analysis of protein concentration determination using biosensor technology under conditions of partial mass transport limitation. Anal. Biochem. **249**, 153–164 (1997)
3. Edwards, D.A.: Estimating rate constants in a convection-diffusion system with a boundary reaction. IMA J. Appl. Math. **62**, 89–112 (1999)
4. Edwards, D.A.: Biochemical reactions on helical structures. SIAM J. Appl. Math. **60**, 1425–1446 (2000)
5. Edwards, D.A.: The effect of a receptor layer on the measurement of rate constants. Bull. Math. Bio. **63**, 301–327 (2001)
6. Edwards, D.A., Goldstein, B., Cohen, D.S.: Transport effects on surface-volume biological reactions. J. Math. Bio. **39**, 533–561 (1999)
7. Edwards, D.A., Jackson, S.A.: Testing the validity of the averaged approximation for the IAsys. Univ. DE Technical Report 2002-3 (2002)
8. Edwards, D.A., Jackson, S.A.: Testing the validity of the effective rate constant approximation for surface reaction with transport. Appl. Math. Lett. **15**, 547–552 (2002)
9. Edwards, P.R., Gill, A., Pollardknight, D.V., Hoare, M., Buckle, P.E., Lowe, P.A., Leatherbarrow, R.J.: Kinetics of protein-protein interactions at the surface of an optical biosensor. Anal. Biochem. **231**, 210–217 (1995)
10. Garland, P.B.: Optical evanescent wave methods for the study of biomolecular reactions. Quart. Rev. Biophys. **29**, 91–117 (1996)
11. Glaser, R.: Antigen-antibody binding and mass transport by convection and diffusion to a surface: A two-dimensional computer model of binding and dissociation kinetics. Anal. Biochem. **213**, 152–161 (1993)
12. Glaser, R.W., Hausdorf, G.: Binding kinetics of an antibody against HIV p24 core protein measured with real-time biomolecular interaction analysis suggest a slow conformational change in antigen p24. J. Immun. Meth. **189**, 1–14 (1996)
13. Goldstein, B., Dembo, M.: Approximating the effects of diffusion on reversible reactions at the cell surface: Ligand-receptor kinetics. Biophys. J. **68**, 1222–1230 (1995)
14. Hall, D.R., Gorgani, N.N., Altin, J.G., Winzor, D.J.: Theoretical and experimental considerations of the pseudo-first-order approximation in conventional kinetic analysis of IAsys biosensor data. Anal. Biochem. **253**, 145–155 (1997)
15. Hoffman, T.L., Canziani, G., Jia, L., Rucker, J., Doms, R.W.: A biosensor assay for studying ligand-membrane receptor interactions: Binding of antibodies and HIV-1 Env to chemokine receptors. Proc. NAS **97**, 11215–11220 (2000)
16. Johnsson, B., Löfås, S., Lindquist, G., Edström, Å., Müller Hillgren, R.-M., Hansson, A.: Comparison of methods for immobilization to carboxymethyl dextran surfaces by analysis of the specific activity of monoclonal antibodies. J. Mol. Recogn. **8**, 125–131 (1995)
17. Karlsson, R., Fält, A.: Experimental design for kinetic analysis of protein-protein interactions with surface plasmon resonance biosensors. J. Immun. Meth. **200**, 121–133 (1997)
18. Karlsson, R., Michaelson, A., Mattson, L.: Kinetic analysis of monoclonal antibody-antigen interactions with a new biosensor based analytical system. J. Immun. Meth. **145**, 229–240 (1991)
19. Lee, M., Rhodes, A.L., Wyatt, M.D., Forrow, S., Hartley, J.A.: GC-base sequence recognition by oligo(imidazolecarboxamide) and C-terminus-modified analogs of distamycin

deduced from circular dichroism, proton nuclear magnetic resonance, and methidium-propyl-ethylene-diaminetetraacetate- iron(II) footprinting studies. Biochem. **32**, 4237–4245 (1993)
20. Liedberg, B., Lundstrom, I., Stenberg, R.: Principles of biosensing with an extended coupling matrix and surface-plasmon resonance. Sens. Actuators B. **11**, 63–72 (1993)
21. Löfås, S., Johnsson, B.: A novel hydrogel matrix on gold surfaces in surface plasmon resonance sensors for fast and efficient covalent immobilization of ligands. J. Chem. Soc. Chem. Commun. **21**, 1526–1528 (1990)
22. Lok, B.K., Cheng, Y.-L., Robertson, C.R.: Protein adsorption on crosslinked polydimethylsiloxane using total internal reflection fluorescence. J. Coll. Int. Sci. **91**, 104–116 (1983)
23. Mason, T., Pineda, A.R., Wofsy, C., Goldstein, B.: Effective rate models for the analysis of transport-dependent biosensor data. Math. Biosci. **159**, 123–144 (1999)
24. Morton, T.A., Myszka, D.G., Chaiken, I.M.: Interpreting complex binding kinetics from optical biosensors: A comparison of analysis by linearization, the integrated rate equations, and numerical integration. Anal. Biochem. **227**, 176–185 (1995)
25. Myszka, D.G., He, X., Dembo, M., Morton, T.A, Goldstein, B.: Extending the range of rate constants available from BIAcore: Interpreting mass transport influenced binding data. Biophys. J. **75**, 583–594 (1998)
26. Parsons, I.D., Stockley, P.G.: Quantitation of the *Escherichia coli* methionine repressor-operator interaction by surface plasmon resonance is not affected by the presence of a dextran matrix. Anal. Biochem. **254**, 82–87 (1997)
27. Raghavan, M., Chen, M.Y., Gastinel, L.N., Bjorkman, P.J.: Investigation of the interaction between the class I MHC-related Fc receptor and its immunoglobulin ligand. Immunity **1**, 303–315 (1994)
28. Schuck, P.: Kinetics of ligand binding to receptor immobilized in a polymer matrix, as detected with an evanescent wave biosensor. I. A computer simulation of the influence of mass transport. Biophys. J. **70**, 1230–1249 (1996)
29. Schuck, P.: Reliable determination of binding affinity and kinetics using surface plasmon resonance biosensors. Curr. Opin. Biotech. **8**, 498–502 (1997)
30. Schuck P., Minton, A.P.: Analysis of mass transport-limited binding kinetics in evanescent wave biosensors. Anal. Biochem. **240**, 262–272 (1996)
31. Stenberg, E., Persson, B., Roos, H., Urbaniczky, C.: Quantitative determination of surface concentration of protein with surface plasmon resonance using radiolabeled proteins. J. Coll. Int. Sci. **143**, 513–526 (1991)
32. Szabo, A., Stolz, L., Granzow, R.: Surface plasmon resonance and its use in biomolecular interaction analysis (BIA). Curr. Opin. Struct. Bio. **5**, 699–705 (1995)
33. Turitto, V.T., Baumgartner, H.R.: Platelet deposition on subendothelium exposed to flowing blood: mathematical analysis of physical parameters. Trans. Am. Soc. Artif. Int. Org. **21**, 593–601 (1975)
34. Wofsy, C., Goldstein, B.: Effective rate models for receptors distributed in a layer above a surface: Application to cells and BIAcore. Biophys. J. **82**, 1743–1755 (2002)
35. Yarmush, M.L., Patankar, D.B., Yarmush, D.M.: An analysis of transport resistance in the operation of BIAcore; implications for kinetic studies of biospecific interactions. Molec. Immun. **33**, 1203–1214 (1996)